ECCOMAS Congress 2016
VII European Congress on Computational Methods in Applied Sciences and Engineering
M. Papadrakakis, V. Papadopoulos, G. Stefanou, V. Plevris (eds.)
Crete Island, Greece, 5–10 June 2016

MODELING THE MECHANICAL RESPONSE OF A LEAD-CORE BEARING DEVICE: DAMAGE MECHANICS APPROACH

T. Zhelyazov[1], **R Rupakhety**[2], **and S. Ólafsson**[2]

[1] Technical University of Sofia, Sofia, Bulgaria
Sofia, 1000, 8 Kl. Ohridski Blvd
e-mail: todor.zhelyazov@tu-sofia.bg

[2] Earthquake Engineering Research Centre, University of Iceland
Austurvegur 2a, 800 Selfoss, Iceland
rajesh@hi.is
simon@hi.is

Keywords: Lead-core Bearing Device, Computational Methods, Damage Mechanics,

Abstract. This paper presents the results of a numerical study aimed at developing a rational approach to assess the degradation of mechanical properties of lead-core bearing devices used for passive seismic isolation. The lead-core rubber bearing is modeled as a multiple-component system. Appropriate constitutive laws and failure criteria are defined for each component of the system. Two alternative constitutive relations are defined for the lead core: bilinear material model by assuming isotropic hardening after yielding, and a model formulated in the framework of continuum damage mechanics. The numerical procedure used to simulate the mechanical response of the device allows the monitoring of accumulated mechanical damage throughout the loading history. Preliminary simulation results obtained by finite element analysis are reported. Specifically, these are shear force-displacement hysteresis loops under various loading conditions in a typical characterization test.

1 INTRODUCTION

The lead-core bearing device is modeled as a multiple-component system. It consists of the following components: lead core, rubber layers, steel shims and thick steel plates. For each material, lead, rubber and steel, an appropriate constitutive law is chosen. The constitutive laws are defined on the meso-scale. At this point, an analogy between the representative volume element in continuum damage mechanics and finite element is postulated. The stress and strain fields in the lead-core bearing device are obtained by finite element analysis on the basis of the postulated constitutive laws. Important macro-characteristics of the bearing can be evaluated throughout the loading history. Such macro-characteristics, if observable, can be employed to calibrate the model or to validate the results obtained by finite element analysis.

2 BEARING DEVICE: SPECIFICATIONS

The geometry of the bearing being modelled and analysed in this study is shown in Figure 1.

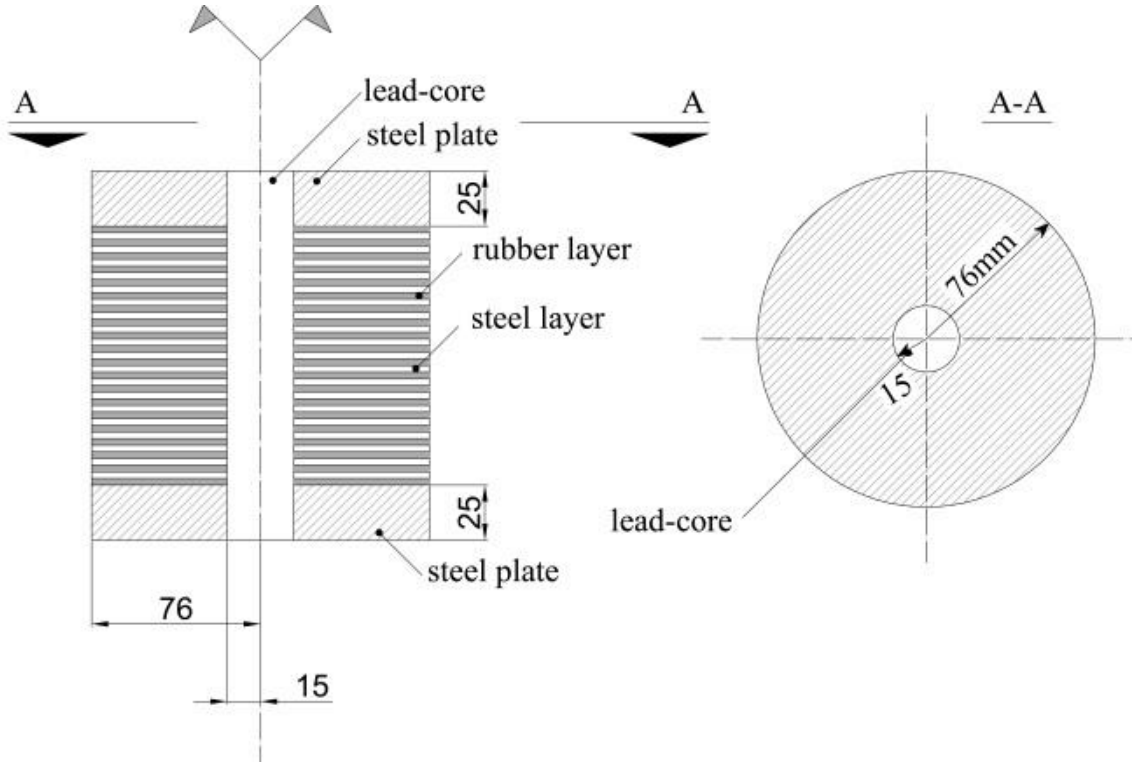

Figure 1: Geometry of the modelled bearing device

As it can be seen, the lead-core bearing device consists of two thick steel plates at the top and at the bottom, rubber layers separated by steel shims, and a lead-core. The thick steel plates are 182mm (2x76) in diameter and 25mm thick with a central cylindrical opening of 30mm diameter. Twenty rubber layers separated by 19 steel shims are stacked between the top and bottom steel plates. The rubber layers and the steel shims are both 182mm in diameter and 3mm thick. They also have a central opening of 30mm diameter along which a lead core of 30mm diameter is fitted.

3 CONSTITUTIVE LAWS

3.1 Steel

Steel is modelled as an isotropic and elastic material. This is justified because, in common usage conditions of the bearing devices, the steel layers and the top/bottom plates remain elastic while yielding occurs in the lead-core and rubber layers. Constitutive law for the steel layers and the top/bottom plates is thus completely defined by initial elastic modulus (Young's Modulus) and Poisson's ratio.

3.2 Lead-core

For the lead-core, a bi-linear stress-strain relationship [1][2][3] is assumed. It is assumed that the material obeys the von Mises yield criterion. An isotropic hardening rule is used to model the post-yielding behavior. As an alternative, a constitutive law based on continuum damage mechanics is formulated, specifically by coupling elasto-palsticity and damage [4]. In this formulation, material response is described by state variables. These variables can be derived form a dissipation potential P that can be written as:

$$P = f + P_X + P_D \tag{1}$$

where f is a function prescribing the yield criterion, P_X describes hardening and P_D represents damage potential [5]. The yield criterion has the following property.

$$\begin{aligned} f < 0 &\rightarrow elasticity \\ f = 0 &\rightarrow plasticity \end{aligned} \tag{2}$$

If both isotropic and kinematic hardening are considered the yield criterion is given by:

$$f = \left(\sigma_{ij} - X\right)_{eq} - R - \sigma_y \tag{3}$$

where

$$\left(\sigma_{ij} - X\right)_{eq} = \sqrt{\frac{3}{2}\left(\sigma_{ij}^D - X_{ij}^D\right)\left(\sigma_{ij}^D - X_{ij}^D\right)} = \left(\sigma_{ij}^D - X_{ij}^D\right)\sqrt{\frac{3}{2}} \tag{4}$$

In equation (4), T_{ij}^D denotes the deviatoric part of a symmetric second order tensor T_{ij}, σ_{ij} is the stress tensor and X is referred to as a back stress (Figure 2).

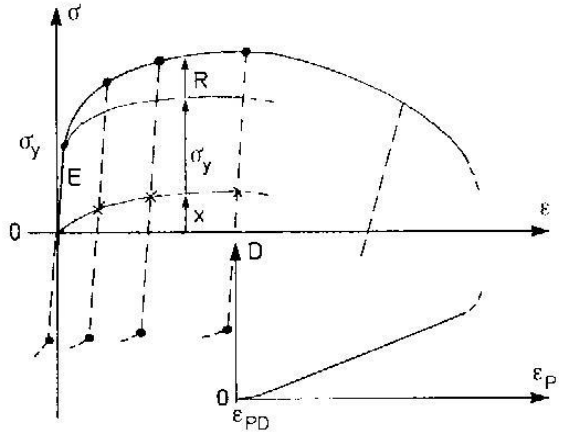

Figure 2: Kinematic back stress X and isotropic hardening stress R [6]

The kinematic back stress X is the locus of the elastic domain center in the stresses space and the isotropic hardening stress R measures the elastic domain increase:

$$R = \sigma - \sigma_y - X \tag{5}$$

The accumulated plastic strain rate is given by the following expression:

$$\dot{p}(t) = \sqrt{\frac{2}{3}\dot{\varepsilon}_{ij}^{p}\dot{\varepsilon}_{ij}^{p}} \tag{6}$$

In (6) $\dot{\varepsilon}_{ij}^{p}$ is the plastic strain rate, obtained after decomposition of the total strain into elastic and plastic part. It is assumed that damage begins when the plastic strain reaches the value corresponding to the ultimate stress (Figure 2) and its critical value is given by:

$$D_c = \left(\frac{\sigma_u^2}{2ES}\right)\left(\varepsilon_p - \varepsilon_{pD}\right) \tag{7}$$

where ε_p is the accumulated plastic strain and ε_{pD} is the plastic strain corresponding to the damage threshold. Damage is accumulated only if $\varepsilon_p > \varepsilon_{pD}$.

$$\begin{aligned} \varepsilon_p > \varepsilon_{pD} &\rightarrow \dot{D} \neq 0 \\ \varepsilon_p \leq \varepsilon_{pD} &\rightarrow \dot{D} = 0 \end{aligned} \tag{8}$$

3.3 Rubber

For rubber, a Neo-Hookean model is used. Strain energy potential is defined by using the following equation.

$$\mathrm{W} = \frac{\mu}{2}\left(\bar{\mathrm{I}}_1 - 3\right) + \frac{1}{\mathrm{d}}\left(\mathrm{J}-1\right)^2 \tag{9}$$

In Eq. (9) μ stands for the initial shear modulus of the material; d is the material incompressibility parameter, and $\bar{I}_1$ is the first invariant of the isochoric part of the right Cauchy-Green deformation tensor. According to [7] and [8], J is the ratio of the deformed elastic volume to the undeformed reference volume of the material. J can be evaluated by calculating the determinant of the Lagrangian strain tensor:

$$J = \det\left[F_{ij}\right] \tag{10}$$

In Eq. (10) F_{ij} denotes the components of the Lagrangian strain tensor. Furthermore, $\bar{I}_1$ can be obtained as

$$\bar{I}_1 = I_1 J^{-2/3} \tag{11}$$

where I_k is the k^{th} invariant of the right Cauchy-Green deformation tensor, and is given by

$$I_1 = \lambda_1^2 + \lambda_2^2 + \lambda_3^2 \tag{12}$$

where λ_i are the principal stretches. The material incompressibility parameter d is related to the material bulk modulus K as follows:

$$K = \frac{2}{d} \tag{13}$$

and the Young's modulus of the material is defined as:

$$E = 2\mu(1+\nu) \tag{14}$$

Based on experimental data, the following values are chosen for the material parameters μ and d [[1]]: μ=0.73MPa and d=0.001mm^2/N.

4 FINITE ELEMENT MODEL

A detailed 3-D finite element model is created. All elements of the bearing device are explicitly modeled in terms of geometry. Volumes are created for the rubber layers, steel shims, the lead-core and the thick top and bottom steel plates. Advantage is taken of the existing symmetries. Only half of the bearing device is modelled. Appropriate symmetry boundary conditions are defined on the plane of symmetry (Figure 3).

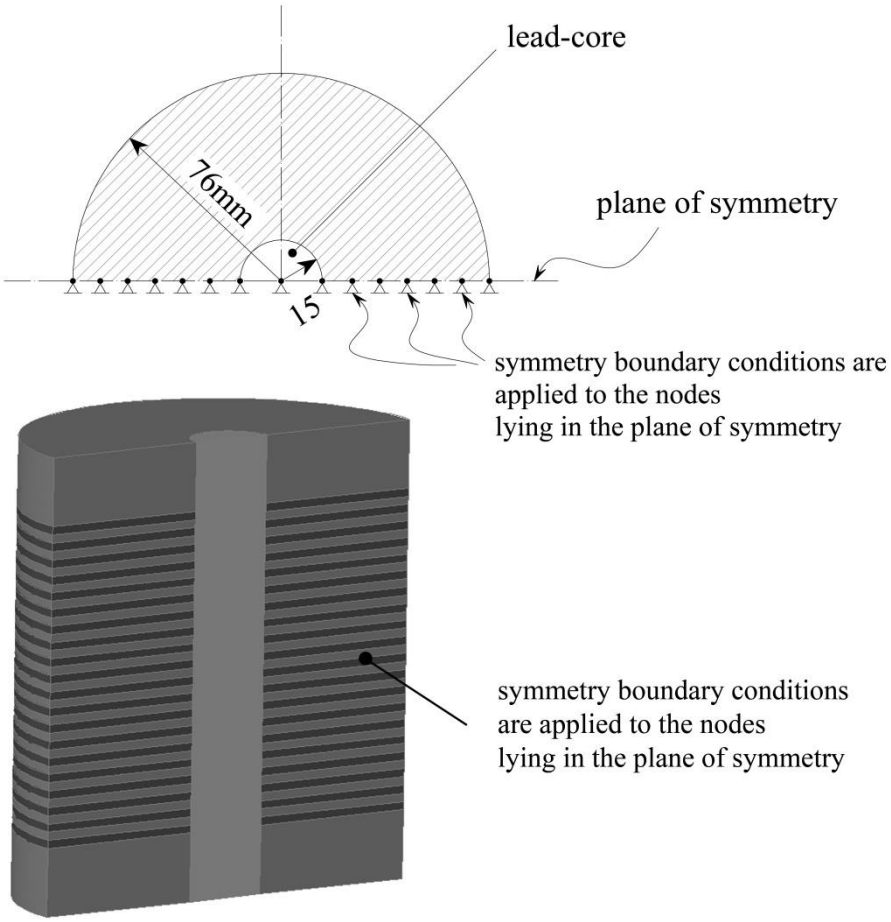

Figure 3: The half-space model and symmetry boundary conditions

For the finite element mesh 20-nodes 3-D structural solids are used (**Figure 4**). Components in steel are meshed with Solid 95 [9]. The lead-core and the rubber layers are meshed with Solid 185 [9]. Full integration option is used to avoid spurious stress hardening.

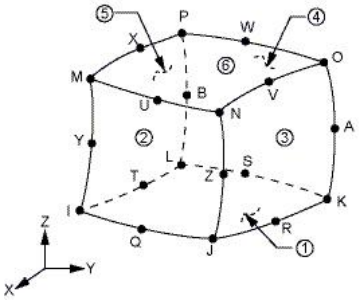

Figure 4: A 20-node 3-D structural finite element [9]

The finite element mesh is displayed in Figure 5. A total of 10290 Solid185 are employed to mesh the volumes of the lead-core, the thick steel plates, the rubber layers and the steel shims. All the interfaces are assumed to give have bonds.

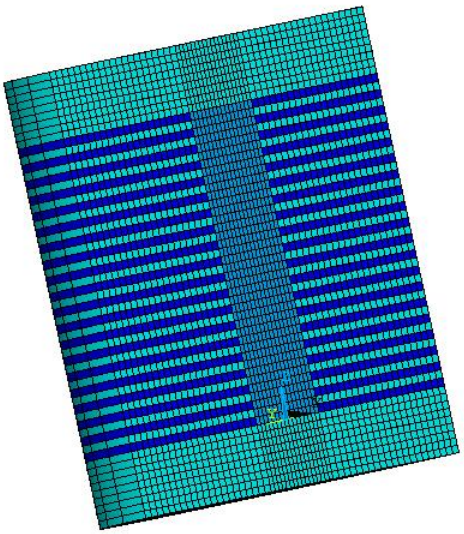

Figure 5: Half-space finite element model: finite element mesh

5 FINITE ELEMENT SIMULATION

The response of the lead-core bearing device is obtained by performing an explicit dynamic transient analysis. The equation of motion has the form:

$$[M]\{\ddot{u}\}+[D]\{\dot{u}\}+[K]\{u\}=\{F(t)\} \tag{15}$$

where [M] is the mass matrix; [D] is the damping matrix; [K] is the stiffness matrix; $\{\ddot{u}\}$ is the nodal acceleration vector; $\{\dot{u}\}$is the nodal velocity vector, and $\{u\}$ is the nodal displacement vector, and $\{F(t)\}$ is the time- dependent loading vector. All the nodes on the 'bottom' surface of the bearing device (Z = -25mm) are restrained against all possible displacements (nodal translations along X-, Y- and Z-axis). Both constant vertical loads and time-dependent horizontal loads are applied to the nodes on the 'top' surface of the bearing device (Z = 142mm). The vertical load is applied along the direction parallel to the global Z-axis in the model space. The time-dependent horizontal load is simulated by applying displacements to the top-surface-nodes in a direction parallel to the global X-axis. The boundary conditions defined for the simulation

of the characterization test are shown in Figure 6. In order to obtain the 'force-displacement' relationship, the evolution of the shear stresses in the lead-core along the global X-direction is monitored.

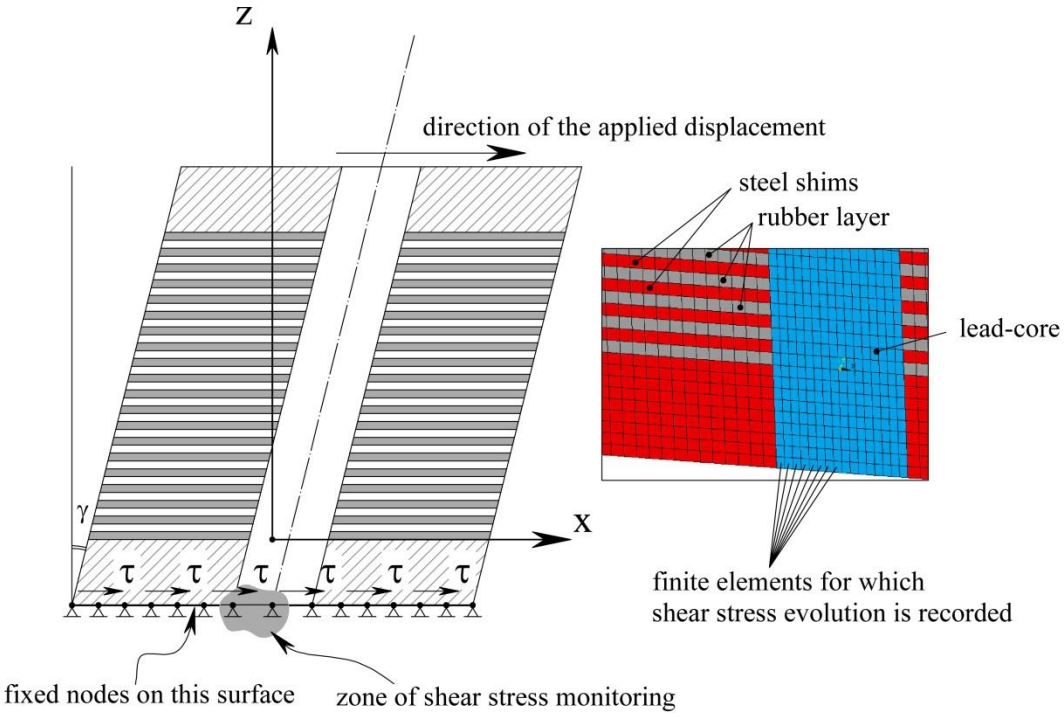

Figure 6: Schematization of the characterization test simulation

The shear strain γ in its turn is conventionally defined as the ratio between the relative horizontal displacement between the top and bottom surfaces of the bearing device- d_h and the total height of the rubber H_r (H_r =60 mm).

$$\gamma = \frac{d_h}{H_r} \tag{16}$$

One of the strain loading paths is visualized in Figure 7.

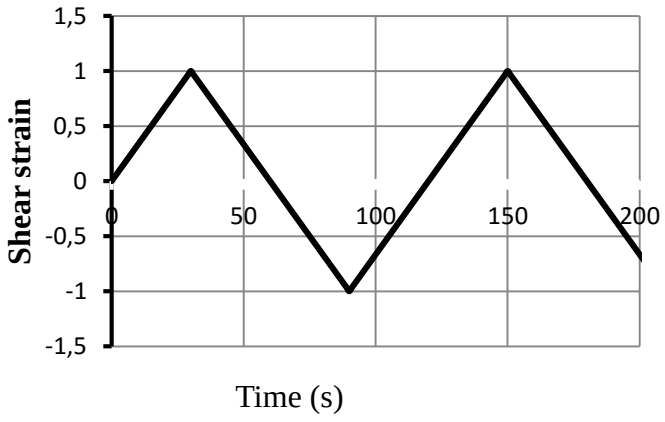

Figure 7: cyclic strain paths

6 RESULTS OBTAINED BY FINITE ELEMENT SIMULATION

In this section shear strain- displacement curves obtained for different shear strain amplitudes and shear strain rates are shown. The numerical procedure reproduces the typical hysteresis behavior exhibited by a bearing device in common identification test. All simulations contain three full hysteresis loops and the ascending branches of the fourth loop. It should be noted that these results should be further validated through comparison with experimental data.

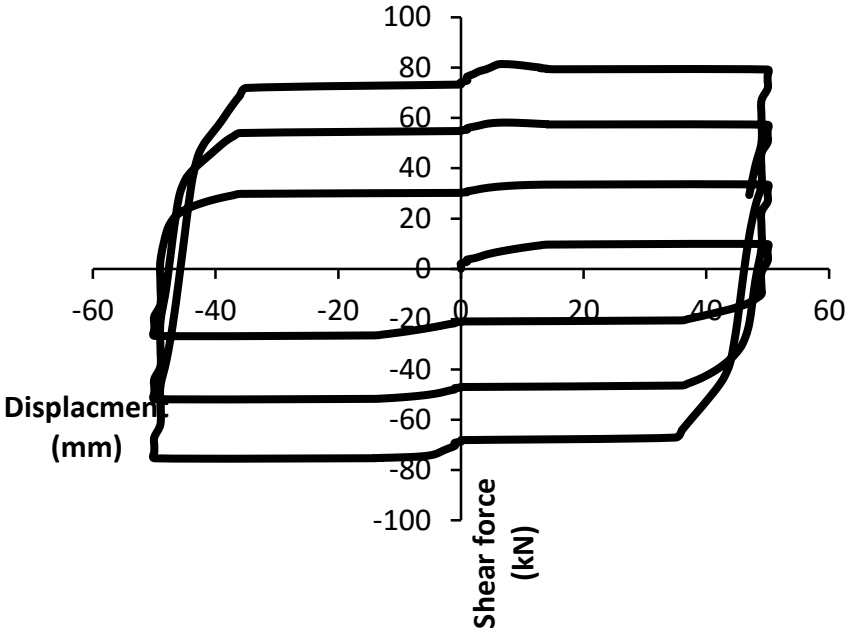

Figure 8: Shear force-displacement hysteresis loops for maximum shear strain γ=0.835 and shear strain rate $d\gamma/dt$=0.083

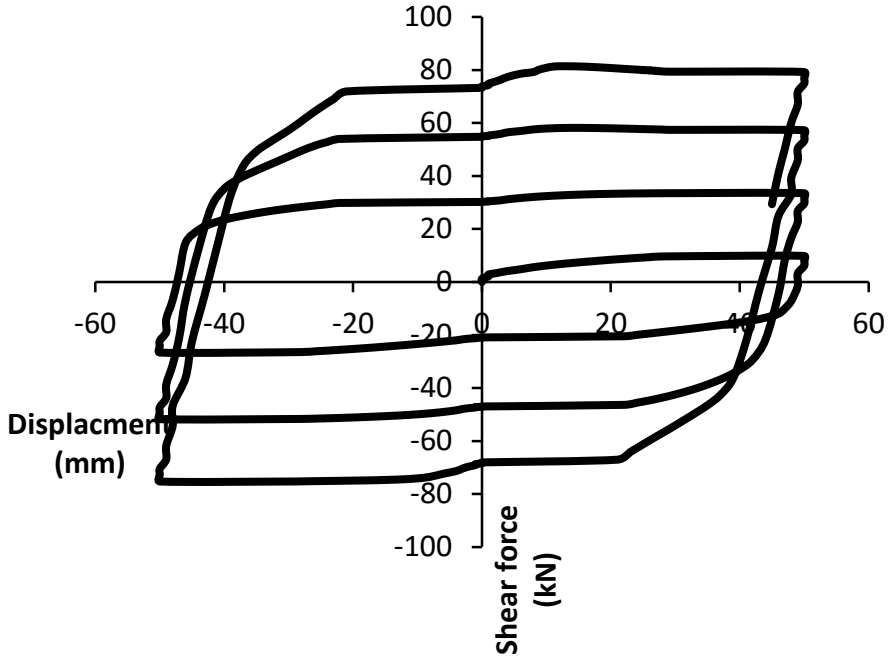

Figure 9: Shear force-displacement hysteresis loops for maximum shear strain γ=0.835 and shear strain rate $d\gamma/dt$=0.042

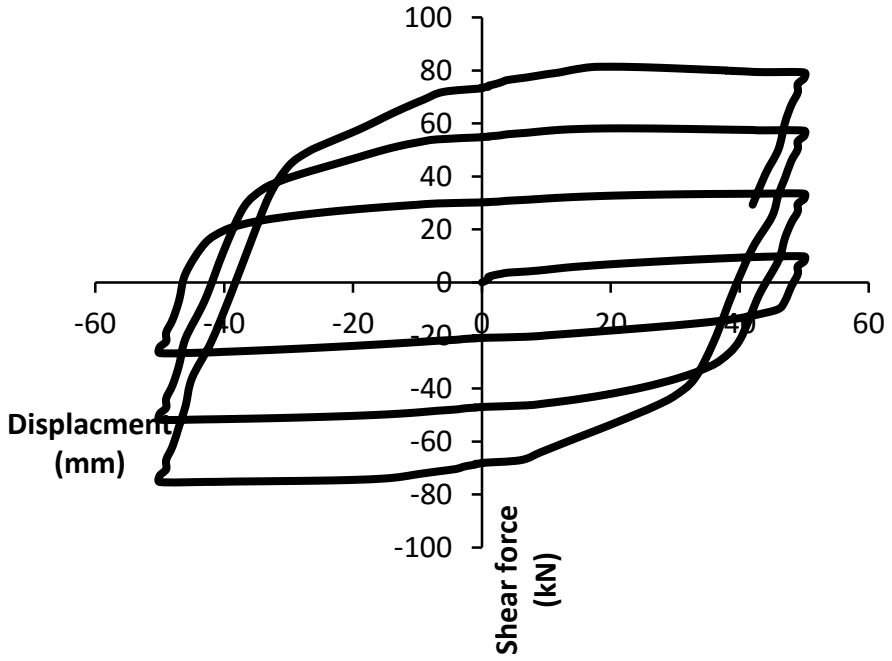

Figure 10: Shear force-displacement hysteresis loops for maximum shear strain γ=0.835 and shear strain rate dγ/dt=0.028

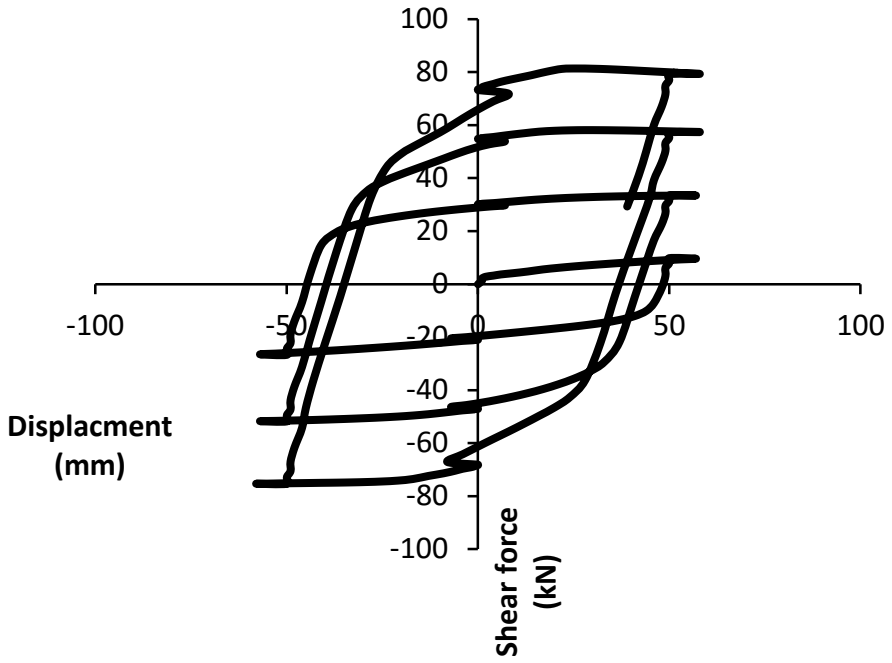

Figure 11: Shear force-displacement hysteresis loops for maximum shear strain γ=0.835 and shear strain rate dγ/dt=0.021

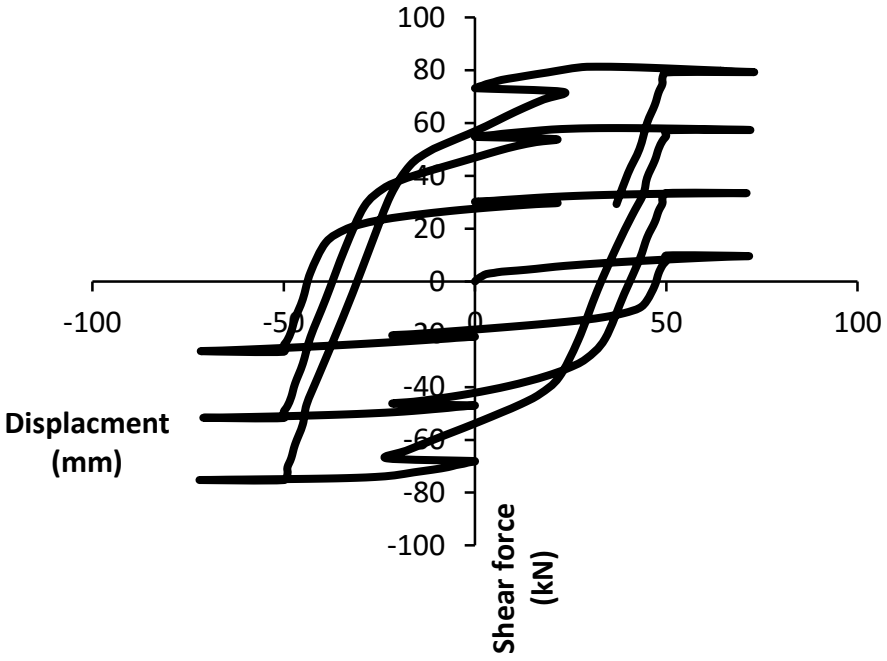

Figure 12: Shear force-displacement hysteresis loops for maximum shear strain γ=0.835 and shear strain rate dγ/dt=0.017

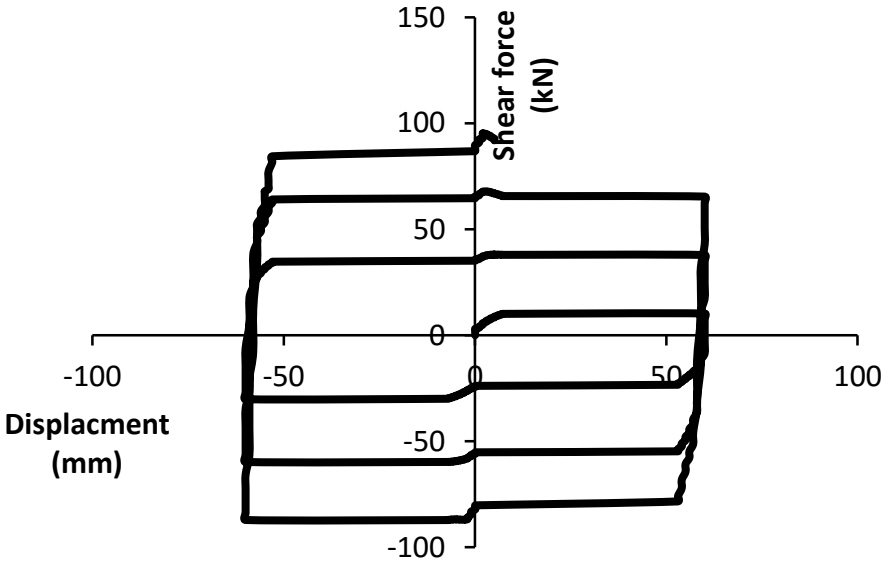

Figure 13: Shear force-displacement hysteresis loops for maximum shear strain γ=1.00 and shear strain rate dγ/dt=0.2

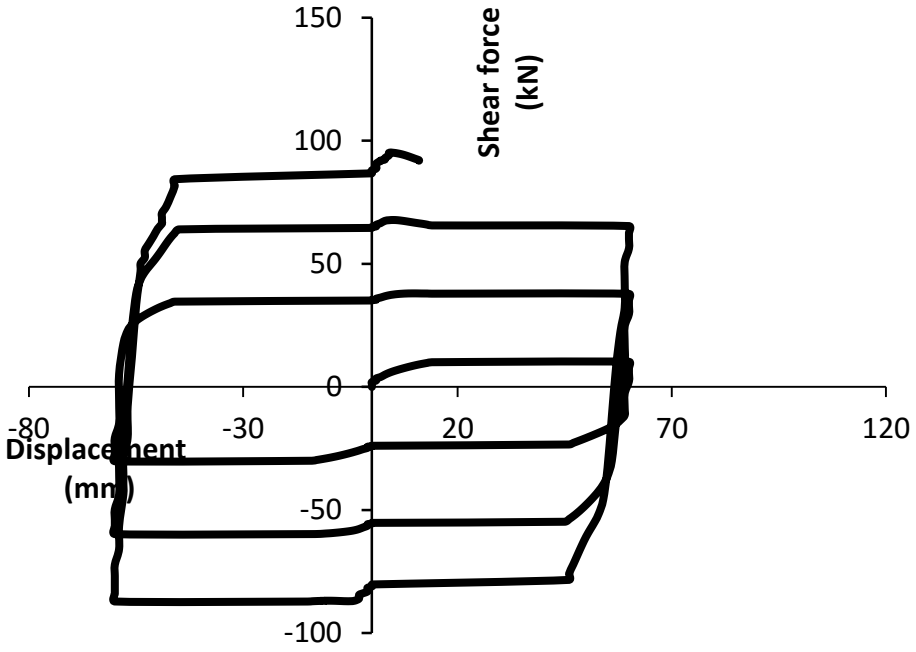

Figure 14: Shear force-displacement hysteresis loops for maximum shear strain γ=1.00 and shear strain rate $d\gamma/dt$=0.1

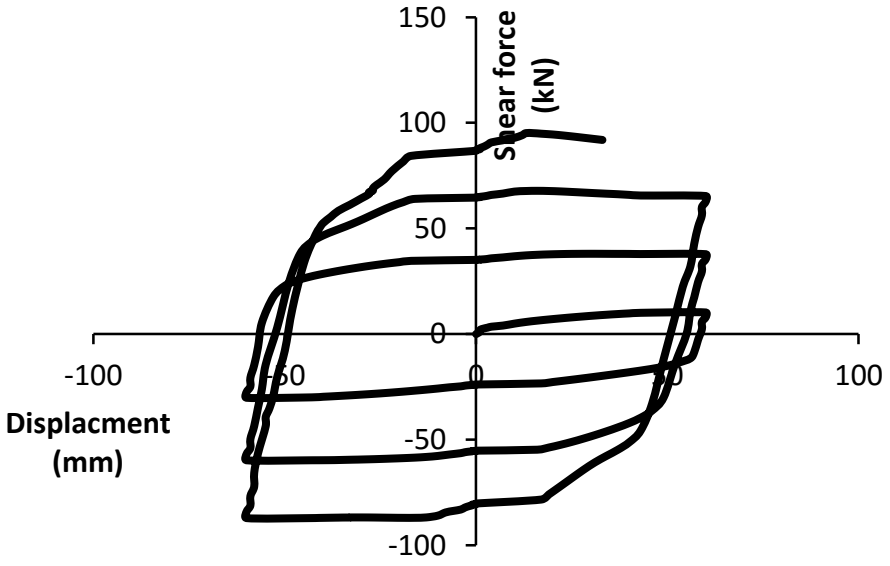

Figure 15: Shear force-displacement hysteresis loops for maximum shear strain γ=1.00 and shear strain rate $d\gamma/dt$=0.033

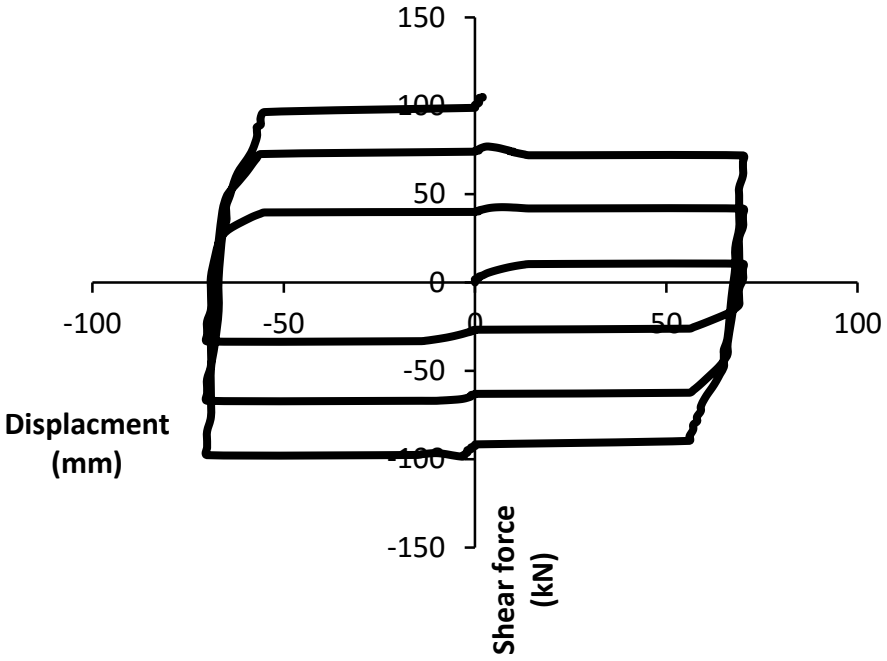

Figure 16: Shear force-displacement hysteresis loops for maximum shear strain γ=1.165 and shear strain rate $d\gamma/dt$=0.117

Qualitative comparison between different 'displacement-shear force' curves obtained by finite element analysis shows that the shear strain rate decrease results in hardening in the ascending branch of each hysteresis loop (compare Figure 8, Figure 9, Figure 10). For further decrease in shear strain rate this trend is conserved. Additionally a sharp discontinuity in the transition between ascending and descending branches as well as at the 'zero-shear strain point' can be observed (see Figure 11 and Figure 12). The latter observation should be addressed again when relevant experimental data is available.

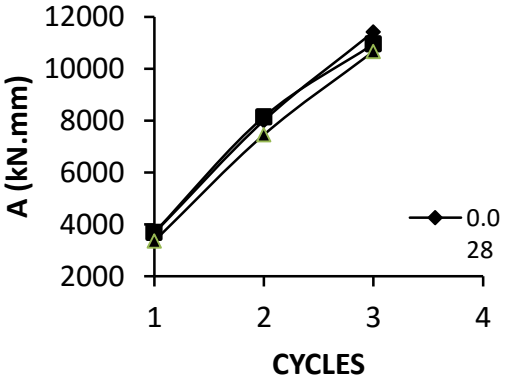

Figure 17: predicted dissipation capacity for different shear strain rates (0.028; 0.021; 0.017)

Furthermore, comparing numerical results obtained for various shear strain rates, it can be concluded that the model predicts a slight decrease in dissipation capacity with the strain rate decrease. This is visualized in Figure 17 which shows an estimate of the dissipation capacity based on results of three finite element simulations. For the three simulations the maximum imposed shear strain is the same whereas the shear strain rate differs.

7 CONCLUSIONS

- This paper presents preliminary results of the study of mechanical response of bearing devices used in passive seismic isolation carried out at the Earthquake Engineering Research Center of the University of Iceland. The study will be further extended by experimental investigation in order to furnish relevant data for model validation.
- Lead-core bearing is modelled as a multiple component system. Appropriate constitutive laws and failure criteria are defined for each material: lead, rubber and steel.
- An explicit and accurate finite element model of a lead-core bearing device is presented. Results obtained by finite element analysis reproduce the hysteresis response of a lead-core bearing device usually exhibited in a common identification test.
- Results obtained by finite element simulation can be further used as a basis for tuning of an analytical differential equation model (curve fitting) aiming a subsequent implementation of the calibrated single-degree-of freedom model into a numerical models of a damped large-scale structures.

REFERENCES

[1] G.P. Warn, K.L. Ryan, A Review of Seismic Isolation for Buildings: Historical Development and Research Needs, *Buildings*, **2(3),** 300-325, 2012.

[2] J. Weisman, G.P. Warn, Stability of Elastomeric and Lead-Rubber Seismic Isolation Bearings, *Journal of Structural Engineering*, 138(2), 215-233, 2012.

[3] G.P. Warn, A.S. Whittaker, A study of the coupled horizontal-vertical behaviour of elastomeric and lead-rubber seismic isolation bearings. *MCEER-06-0011, Multidisciplinary Center for Earthquake Engineering Research*, Buffalo, New York 2006.

[4] J. Lemaitre, Coupled Elasto-Plasticity and Damage Constitutive Equations, *Computer methods in Applied Mechanics and Engineering*, 51, 31-49, 1985

[5] J. Lemaitre, R. Desmorat, *Engineering damage mechanics*, Springer-Verlag Berlin Heidelberg, 2005.

[6] J. Lemaitre, *A Course on Damage mechanics*, Springer, Berlin Heidelberg, New York, 1996.

[7] R.W. Ogden, *Nonlinear Elastic Deformations*, Dover Publications, Inc., 1984.

[8] M.A. Crisfield, Non-linear Finite Element Analysis of Solids and Structures, Vol. 2, Advanced Topics, John Wiley & Sons, 1997.

[9] ANSYS Mechanical APDL Element Reference

[10] T. Zhelyazov, E.R. Thorhallsson, Simon Ólafsson, J.T. Snæbjörnsson, R. Sigbjörnsson, Seismic isolation: assessment of the damping capacity, *Second European Conference on Earthquake Engineering and Seismology*, Istanbul, August 25-29, 2014.